Preparation and Application of Monodispersed Mesoporous Submicron Carbon Particles as a Drug Carrier

Shou-Cang Shen[1]*, Wai Kiong Ng[1], Leonard S.O. Chia[1], Yuan-Cai Dong[1], Reginald B. H. Tan[1,2]*

[1] Institute of Chemical and Engineering Sciences, A*STAR (Agency for Science, Technology and Research), 1 Pesek Road, Jurong Island, Singapore 627833.

[2] Department of Chemical and Biomolecular Engineering, The National University of Singapore, 4 Engineering Drive 4, Singapore 117576

* corresponding author: Tel: +65 6796 3841; Fax: +65 6316 6188;

E-mail: reginald_tan@ices.a-star.edu.sg; shen_shoucang@ices.a-star.edu.sg

Abstract

Monodispersed mesoporous carbon (MMPC) submicron carbon particles have been fabricated by co-spray drying of SBA-15 submicron particles and sucrose, followed by carbonization in a nitrogen environment and removal of the hard SBA-15 template in NaOH solution. The ratio of sucrose/SBA-15 used for the co-spray drying affected the integration and dispersibility of the obtained mesoporous carbon particles and sucrose/SBA-15 ratios at 1.0 ~1.5 resulted in monodispersed mesoporous carbon submicron particles. The surface properties of MMPC could be modified by treatment in nitric acid solution to create oxygen groups and thus increase wettability of MMPC powder. MMPC particles were used as drug carrier to enhance the dissolution rate of a poorly soluble drug, indomethacin (IDMC) *via* co-spray drying. The morphology of MMPC was not changed after drug loading as most IDMC molecules were encapsulated into its pore channels in amorphous state, which was characterized by X-ray diffraction (XRD) and differential scanning calorimetry (DSC). Due to the ordered mesoporous structure, the pore walls separate the IDMC particles and prevent recrystallization from happening. The amorphous IDMC/MMPC solid dispersion exhibited excellent stability under stress storage conditions of 40 °C/75 %RH for six months. The amorphous formulation contributed to the significantly enhanced dissolution rate of IDMC from solid dispersion.

Keywords: Monodisperse, mesoporous carbon, drug carrier, spray drying

1. Introduction

Since the discovery of mesoporous silica, many mesoporous materials have been synthesized for various applications involving large molecules or for biomolecular engineering, which was achieved by using conventional microporous zeolitic materials [1-4]. Among these mesoporous materials, ordered mesoporous carbons with various pore structures have mainly been synthesized by nano-casting technology using appropriate ordered mesoporous silica as hard templates. They have been successfully fabricated and modified for potential applications as catalysts [5-8], adsorbents[9], separation media[10], energy storage [11-15] and advanced electronic materials [16] in many scientific disciplines [17] since Ryoo *et al.* reported the synthesis of CMK-1 mesoporous carbon [18]. Among the various applications, the utilization of mesoporous carbon as drug carriers have attracted much attention as they have shown great potential applications in drug formulation because of their well-ordered pore structure, very high specific pore volume, specific surface area, tunable pore diameter and biocompatibility [19, 20]. The large surface area to volume ratio of these nanostructured materials provides the potential for significant drug loading through surface adsorption [21]. Mesoporous carbon materials are also highly tolerant in aqueous environments as compared to silica materials. The stable nanostructures of mesoporous carbon could ensure that it preserves their drug cargo in the body to enable effective targeting and release at the diseased site [22,23]. Gu *et al.* [24] applied mesoporous carbon as carriers for the delivery of hydrophobic anti-cancer drug, camptothecin, which efficiently inhibited the growth of MCF-7 cancer

cells due to its sustained release. Wang *et al.* [25] reported that ibuprofen loaded on mesoporous carbon exhibited a two-step release profile of an initially fast release followed by a slower release. Zhao *et al.* [26] found that mesoporous carbon could achieve a higher degree of drug loading and dissolution of poorly soluble drugs could be markedly increased. Moreover, mesoporous carbon exhibited a weak cytotoxicity at tested concentrations (10–800 μg/ml). Labiano *et al.* [27] studied the slow release kinetics of mitoxantrone from ordered mesoporous carbon films where the high porosity and surface areas of ordered mesoporous materials provide substantial capacity for the loading of guest molecules, and could achieve a controlled release.

The preparation of mesoporous carbon usually uses mesoporous silica as the hard template and followed by a replication process. The harvested mesoporous carbon generally preserves the morphology of mesoporous silica [17]. Most mesoporous carbon materials usually exhibit the common fiber morphology although various pore structures were fabricated [28-31]. To our best knowledge, mono-dispersed mesoporous carbon materials have rarely been reported. In this study, sucrose was filled to mesoporous silica by a co-spray drying process at different ratios of sucrose/SBA-15. Following carbonization in a nitrogen environment and subsequent removal of the hard SBA-15 template by NaOH, the obtained monodispersed mesoporous carbon were used as drug carriers for loading a poorly soluble drug, IDMC to improve IDMC's dissolution rate and bioavailability. The drug loading performance of MMPC was compared with porous activated carbon (AC) with non-uniform pore structures and non-porous microspheres of carbon (MSC). The molecular state of drug in the IDMC/MMPC solid dispersion was studied by scanning electron microscopy (SEM), DSC, XRD and N_2 adsorption.

2. Materials and Methods

2.1. Synthesis of mesoporous submicron particles

Mesoporous SBA-15 with submicron particle size was synthesized by a rapid condensation process. 4.0 g of template, EO_{20}-PO_{70}-EO_{20} (P123, pluronic 123, Aldrich) was dissolved in 150 g of a 2 N HCl solution under stirring at 40 °C for 2 h. 8.5 g of Tetraethylorthosilicate (TEOS, Aldrich, 98%) was added to the solution under vigorous stirring for 2 min. The hydrolysis of TEOS was performed at 40 °C for 2 h without stirring for different periods. The mole ratio of components in the mixture is SiO_2 : P123 : HCl : H_2O = 1.0 : 0.016 : 6.9 : 178.6. The mixture was transferred to a polypropylene bottle and aged in an oven at 100 °C for 24 h. The resulting material was filtered and washed with deionized water, then dried at 55 °C for 12 h. To remove the template molecules, the material was heated from room temperature to 550 °C for 6 h in air at a heating rate of 2°C/min.

2.2. Preparation of Monodisperse Mesoporous Carbon

Monodispersed mesoporous carbon was prepared by using submicron SBA-15 as hard templates and sucrose was used as the carbon precursor. Sucrose was filled to mesoporous structure of SBA-15 by co-spray drying process. Typically, 1.0 g of sucrose was dissolved in a mixed solvents of 80 ml of methanol and 20 ml of water as well as 0.18 g of H_2SO_4 (98%). The 1.0 g of SBA-15 submicron particles was mixed with sucrose solution under stirring. The suspension was co-spray dried with a mini spray dryer (BÜCHI B-290, BÜCHI Labortechnik AG, Flawil, Switzerland) operated with an inlet temperature of 68 °C and feeding rate of 4 ml/min. Carbonization experiments were performed with a tubular furnace in purified N_2 flow at 900 °C for 6 h and a heating rate of 10 °C/min. The obtained carbon–silica composite was washed with 1 M NaOH solution of 50% ethanol-50% H_2O twice at 90 °C, in order to

dissolve the silica template followed by washing with de-ionized water to remove trace NaOH completely. Four mesoporous carbon samples were prepared by co-spray dried sucrose/SBA-15 with ratios of 0.5, 1.0, 1.5 and 2.0, and the resulting MMPC was denoted as MMPC-1, MMPC-2, MMPC-3 and MMPC-4, respectively.

2.3. Nitrogen adsorption

Nitrogen adsorption/desorption isotherms were measured by using a gas adsorption analyzer (Autosorb-6B, Quantachrome Instruments, Boynton Beach, FL, USA) at a temperature of –196 °C. Before nitrogen adsorption-desorption measurements, each sample of monodisperse mesoporous carbon was heated at 100 °C under vacuum overnight. For samples of drug loaded carbon, each sample was degassed at 40 °C under vacuum overnight. The specific surface areas of the samples were determined from the linear portion of the Brumauer-Emmett-Teller (BET) plots. The mesoporous carbon pore size (diameter DBET) distribution (with and without drug loading) was calculated from the desorption branch of N_2 adsorption-desorption isotherms using the conventional Barrett-Joyner-Halenda (BJH) method. The total pore volume, V_T, was estimated from the amount adsorbed at a relative pressure of 0.95.

2.4. Scanning electronic microscopy

The morphology of monodisperse mesoporous carbon was examined by high resolution field emission scanning electron microscopy (FESEM, JSM-6700F, Jeol Ltd., Tokyo, Japan). Samples were loaded and adhered to double faced carbon tape on the sample stub then sputter coated with gold by a sputter coater (High Resolution Sputter Coater 208HR, Cressington Scientific, Watford, UK). The SEM was operated with an accelerating voltage of 5 kV and specimen working distance of 8 mm.

2.5. Transmission electron microscopy

The morphology and structures of mesoporous carbon were also examined by transmission electron microscopy (TEM, G2 F20, Tecnai, Hillsboro, OR, USA) at 200 kV. The specimens for high resolution transmission microscopy (HRTEM)/TEM/selected area electron diffraction (SAED) studies were prepared by suspending a solid sample in acetone with ultrasonic dispersion in a water bath.

2.6. Fourier transform infrared spectroscopy

The framework vibration Fourier transform infrared (FTIR) spectra were recorded on an infrared spectrophotometer (Bio-Rad, TFS 3000MX, Hercules, CA, USA) at a resolution of 2 cm^{-1}. The samples were thoroughly ground with KBr pellets before being pressed at 4 ton to form a thin wafer.

2.7. Raman spectroscopy

The Raman scattering spectra were measured at room temperature using a Raman microscope (JY LabRAM, Horiba Ltd., Kyoto, Japan) equipped with liquid-nitrogen-cooled charge-coupled device (CCD), multichannel detector (256 pixels × 1024 pixels) and a high grade Olympus microscope (objective 100×). The spectra were recorded using the visible 514.5 nm argon ion laser as the scattering excitation source. The laser power on the sample was about 6 mW. The spectral acquisition time for each Raman spectrum was about 120 s with spectral resolution around 1.5−2 cm^{-1}.

2.8. Chemical oxidation of MMPC

To introduce oxygen-containing functional groups on the surface of MMPC, MMPC-3 was selected to be oxidized by nitric acid. 1.0 g of MMPC-3 was treated

with treated with 100 ml of 4M HNO_3 solution for 3 h at a temperature of 80 °C. After oxidation, samples were recovered and washed thoroughly with ultra pure water until the pH was close to 7.0, and further dried at 90 °C overnight.

2.9. Water Vapor dynamic adsorption and desorption

Sorption isotherms of MMPC-3 and MMPC-3-OX were obtained using dynamic vapor sorption (DVS Advantage, Surface Measurement Systems, Alperton, UK). The humidity range was varied from 0 %RH to 90% RH in steps of 10% RH at 40 °C. The instrument was run in dm/dt mode to decide when equilibrium had been reached, with a reported 33 dm/dt set at 0.002 %RH/min within an interval of 5 min. Approximately 10–12 mg of sample was used for each run.

2.10. Differential scanning calorimetry

Differential scanning calorimetry (DSC) was performed concurrently using a simultaneous TGA-DSC thermogravimetric analyzer (SDT 2960, TA Instrument Co., New Castle, DE, USA). Ten mg of sample was used in each experiment. The sample was heated from room temperature to 200 ^{o}C under nitrogen flow of 100 mL/min with a heating rate of 10 ^{o}C/min

2.11. Drug loading

One gram of indomethacin was dissolved in 100 mL of ethanol and one gram of mesoporous carbon or other types of carbon was dispersed in the solution under stirring. The spray drying was performed on a BÜCHI B-290 mini spray dryer (BÜCHI Labortechnik AG, Switzerland) operated in inert loop mode. The inlet temperature was set to 81 °C and the resulting outlet temperature at the above-mentioned operating conditions was approximately 50-55 °C. The feed rate was 4.0

mL/min. The loading of IDMC in resulted solid dispersion was assayed by extraction with pH 6.8 PBS buffer under stirring at 50°C overnight. After filtrated with micro-filter (0.45μm), the concentration of IDMC was measured by UV spectrometer at wavelength of 320 nm. The efficiency of encapsulation was calculated according to the ratio of measured drug loading to designed value.

2.12. In Vitro Drug Release Studies.

The dissolution profile of indomethacin from solid dispersion was measured using VK7010 (Varian Co) USP dissolution tester (Varian VK7010 Dissolution Apparatus, Varian Inc., Palo Alto, CA, USA) with online flow cell (Cary 50 UV-visible spectrophotometer, Varian Inc., Palo Alto, CA, USA). The stirring rate was set at 100 rpm and the vessel temperature at 37 °C. Typically, 58 mg of spray-dried co-spray dried IDMC with MMPC (drug loading 43.4 wt.%) and 25 mg of pure indomethacin (Sigma) crystal were used for dissolution testing in 900 mL of pH 6.8 phosphate buffer at 37 ºC. Samples were taken by the auto sampling system equipped with filters at intervals of 5 min. After each measurement, liquid samples were conveyed back to the dissolution vessel by a peristaltic pump. UV readings were taken at a wavelength of 320 nm. For tablet dissolution tests, 58 mg of spray-dried IDMC/MMPC powder was mixed with 800 mg of corn starch and pressed to tablet (13 × 6 mm) at a pressure of 75 mPa.

2.13. Powder X-ray Diffraction

Powder X-ray diffractograms were obtained for the co-spray dried particles using an X-ray diffractometer (D8 ADVANCE, Bruker Corporation, Madison, WI, USA) in steps of 0.02^{o} using Cu Kα radiation as the X-ray source. The

measurement conditions were as follows: target, Cu; filter, Ni; voltage, 40 kV; current, 10 mA; scanning speed, 2^{o}/min

3. Results and Discussion

Figure 1A displays the nitrogen adsorption and desorption isotherms of MMPC samples prepared by using different ratios of sucrose/SBA-15. All MMPC samples exhibited the typical Type IV isotherm curves with distinct capillary condensation steps at a P/P_0 range of 0.4 ~ 0.7, indicating ordered mesoporous materials with narrow pore size distributions. Figure 1B shows the pore size distribution peak of MMPC samples. Sample of MMPC-1 exhibited a sharp pore size distribution peak at 3.8 nm, while the pore size of MMPC slightly shifted to 3.4 nm with the increase of the ratio of sucrose/SBA-15. For MMPC prepared with a sucrose/SBA-15 ratio at 0.5, the pore channels of SBA-15 were not fully filled and partial interstitial gap between silica and sucrose could attribute to the pore space of resulting MMPC materials. For MMPC prepared with a sucrose/SBA-15 ratio below 2.0, the original pore channels of SBA-15 were completely filled and no interstitial gaps could contribute to the pore space of the resulting MMPC after carbonization and remove of silica pore wall, thus the pore size is slightly smaller. Table 1 lists the specific areas and pore properties of MMPC samples. For the sample prepared with a sucrose/SBA-15 ratio of 0.5, MMPC-1, has a specific surface of 1100 m^2/g and total pore volume of 1.09 cm^3/g. With increase of the sucrose/SBA-15 ratio to 1.0 - 2.0, the obtained MMPC samples exhibited similar surface areas about 1800 m^2/g, meanwhile the total pore volume was also increased and MMPC-3 prepared at a sucrose/SBA-15 ratio of 1.5 possessed the largest pore volume of 1.82 cm^3/g.

Figure 2 displays the SEM images of MMPC samples. The morphologies of resultant mesoporous carbon generally replicated the morphology of submicron particles of mesoporous silica used as templates. For the sample prepared with a sucrose/SBA-15 ratio of 0.5, the particle surface exhibited a fiber-stack-like surface and carbon fibers were also observed. As the mesoporous structure of SBA-15 was not fully filled, carbon fibers were formed in the pore channels of SBA-15 after carbonization and removal of the silica framework, and cannot be held as part of the integrated particle as observed in the high magnification SEM image inset of MMPC-1. This effect also resulted in the smallest pore volume and specific surface areas among samples prepared in this study (Table 1). For mesoporous carbon fabricated with a sucrose/SBA-15 ratio above 1.0, part of the sucrose remained on surface of SBA-15 after co-spray drying and facilitated the assembly of mesoporous carbon after carbonization. The surface of submicron carbon particles are smooth and agglomeration of mesoporous carbon particles for MMPC-4 was observed. The morphology and pore structure of monodispersed mesoporous carbon was also investigated by TEM (Figure 3). The TEM image indicates that MMPC-1 comprised of broken particles as the carbon source was not sufficient to be held together after removal of the mesoporous silica template. For MMPC-2 and MMPC-3 fabricated with sucrose/SBA-15 ratios of 1.0 or 1.5, the particles exhibited integration and good monodispersion. When the sucrose/SBA-15 ratio was increased to 2.0, the sucrose remaining on the external surface of SBA-15 formed carbon to bind the mesoporous carbon to large agglomerates. The high resolution TEM images of MMPC-3 and MMPC-4 indicate that the monodispersed mesoporous carbon possessed a highly ordered 2-dimensional (2-D) pore structure.

Figure 4 displays the Raman spectra of MMPC-2 and MMPC-3 mesoporous carbon submicron particles with good mono-dispersion. The results indicate that carbonization at 900 °C led to the formation of graphite structures. All samples show the typical peaks of carbon materials at 1350 and 1585 cm^{-1}. The peak at about 1585 cm^{-1} (G band) is attributed to an E_{2g} mode of hexagonal graphite and is related to the vibration of sp^2-bonded carbon atoms in a graphite layer, and the D band at about 1350 cm^{-1} is associated with the vibration of carbon atoms with dangling bonds in the plane terminations of disordered graphite. The relative intensity ratio of D to G band, I_D/I_G, can be related to the degree of graphitization [32]. The similar intensity of D and G bands indicated that the mesoporous carbon materials were composed of some small graphite sheets with structural defects and the two samples showed the similar graphitization degree after carbonization at 900 °C.

The surface groups of original monodispersed mesoporous carbon and chemically oxidized MMPC were analyzed by FT-IR spectroscopy (Figure 5). It can be seen that, compared with the original MMPC, several new peaks were observed to be created after treatment with nitric acid. The absorption band at 1352 cm^{-1} is attributed to nitro ($-NO_2$) stretching vibration and carbonyl groups (-C=O) contributed to the stretching vibration at 1712 cm^{-1}. The broad band at 3200 – 3600 cm^{-1} is assigned to stretching vibration of hydroxyl groups [33]. These newly formed IR absorption bands indicate that oxygen-containing groups, such as nitro, hydroxyl, carboxylic, lactones and ketene, are created on the modified ordered mesoporous carbons by the oxidation of surface carbon species [34]. The modification of the surfaces of mesoporous carbon with functional groups is expected to change its hydrophobic properties and increase its wettability.

The wettability of MMPC-3 was investigated by dynamic vapor adsorption and Figure 6 shows the water adsorption-desorption isotherms of MMPC-3 before and after oxidation treatment. The results indicated that the original MMPC-3 showed low level of water uptake. At P/P_0 of 0.6, only 7% (w/w) of water vapor adsorption was observed and 38% (w/w) water adsorption at P/P_0 of 0.9. By comparison, modified MMPC-3 showed substantial water uptake at P/P_0 from 0.1 to 0.5 where the original MMPC-3 showed very low level uptake of water. At P/P_0 of 0.6, 34.7% (w/w) of water uptake was achieved on modified MMPC-3. The oxidized MMPC-3 exhibited a much high capability for water adsorption due to its improved hydrophility of surface functional groups, and the existence of the functional groups is also expected to change the adsorption/desorption of other organic ingredients.

The modified MMPC-3 was used as a drug carrier to be co-spray dried with a model poorly soluble drug, indomethacin (IDMC). In this study, non-porous microspheres of carbon (MSC) and porous active carbon (AC) with a non-uniform pore structure were also used as a comparison to investigate drug loading performance. Figure 7 exhibits the morphology transformation of various carbon materials after the co-spray drying with indomethacin at IDMC/carbon ration of 1:1 (w/w). It can be seen that, the morphology MMPC-3 was not obviously changed after co-spray drying with IDMC, implying that most IDMC was entrapped inside the mesoporous structures. Even if part of the IDMC molecules has not been entrapped into pore channels *via* capillary condensation, the IDMC remaining on the external surface was not observed to form new particles. The encapsulation efficiency of IDMC/MMPC (1:1) is 86.8% based on the ratio of measured drug loading to designed value. From Figure 8, N_2 adsorption measurements indicate that the total pore volume of modified MMPC-3 was reduced from 1.33 to 0.35 cm^3/g. As a comparison, when non-porous

carbon MSC was used as a drug carrier, the morphology of the co-spray dried solid was obvious changed after loading with IDMC. As the total pore volume of MSC is only 0.03 cm^3/g, there is no porous structure to accommodate IDMC molecules and most IMDC molecules played the role as binder at the external surface to agglomerate MSC particles. However, although the porous AC particles have plenty of porosity for entrapment of IDMC molecules, extra particles could be observed to be formed on the external surface of AC after spray drying. As the pore structure of AC is not uniform as MMPC, the capillary condensation of IDMC solution is not smooth during the rapid drying of the spray drying process and left more IDMC molecules on the external surface of AC to form new needle-like particles. After co-spray drying with IDMC, the total pore volume of the solid dispersion was 0.43 cm^3/g while that of AC was 1.16 cm^3/g. The results also implied that partial amounts of IDMC were entrapped in the pore structure of AC and occupied the pore volume although some particles of IDMC were formed at the external surface of AC.

Figure 9 displays DSC curves of solid dispersions of IDMC co-spray dried with different drug carriers and compared with pure IDMC crystals. The untreated IDMC crystal exhibited a strong endothermic peak at 160 °C, which corresponds to the melting of the IDMC crystal. By comparison, IDMC co-spray dried with MSC showed doublet endothermic peaks at 152 and 158 °C, indicating that IDMC is not uniformly dispersed among the particles of MSC. The solid dispersion of IDMC co-spray dried with AC exhibited a weak endothermic peak at 150 °C. However, these endothermic DSC peaks were not observed for IDMC co-spray dried with MMPC, implying that the solid dispersion of IDMC entrapped in MMPC is amorphous. According to a reported investigation of crystallization processes in confined spaces, crystallization can only occur in channels with diameter to molecular size ratios above

20 [35, 36]. The pore diameter in this study was about 3.8 nm, which is smaller than five times of the dimension of the indomethacin molecule (estimated to be about 1 nm). The limited size of the mesoporous channels prevents the formation of crystalline indomethacin.

Figure 10 shows the dissolutions profiles of co-spray dried IDMC and MMPC and compared with pure untreated IDMC crystals. The dissolution of IDMC/MMPC was conducted both in powder and tablet forms. It was found that the dissolution rate of co-spray dried IDMC/MMPC powder was much faster than that of pure IDMC crystals. As the MMPC drug carrier was modified with oxygen-containing groups on surface and possessed better wettability, the powder form IDMC/MMPC solid dispersion could be quickly dispersed in the dissolution medium and reduced the floating period of powder. Consequently, IDMC dissolved from the solid dispersion of IDMC-MMPC rapidly reached about 70% dissolution in 5 min and achieved about 80% in 15 min. As a comparison, the untreated IDMC crystal was only dissolved about 6% in first 5 min and achieved 28% dissolution in 15 min. Although the tablet pressed with corn starch took a while to disintegrate, IDMC from solid dispersion tablets also achieved 74% dissolution in 5 min. The disintegrated tablet facilitated the particles to be fully dispersed into medium and even exhibited better burst dissolution than the powder form. The rapid dissolution of IDMC from the solid dispersion is attributed to the completely amorphous state of IDMC entrapped inside the mesoporous structure [37,38]. Nevertheless, it was observed that after about 80% dissolution of IDMC/MMPC solid dispersion was quickly achieved in 15 min, the dissolution also achieved an equilibrium level. This incomplete dissolution was also reported for the loading of other active pharmaceutical ingredients (APIs) using mesoporous carbon as carriers [26, 39, 40]. The adsorption of IDMC on the internal

surface of micropores could result in the incomplete dissolution of IDMC from solid dispersion of IDMC/MMPC.

Figure 11 illustrates the XRD patterns of co-spray dried IDMC with modified MMPC powders after storage under severe stress test conditions of 40 °C/75 %RH in open pans for different periods. As the improved dissolution rate of IDMC/MMPC solid dispersions obtained by co-spray drying is attributed to the amorphous state of IDMC formed in the pores channels of MMPC, the stability of the amorphous state during storage is a crucial property to assess the applicability of the formulations. It was found that the amorphous form of IDMC co-spray dried with MMPC exhibited excellent stability against re-crystallization at the accelerated stressed test conditions of 40 °C/75 %RH. As shown in Figure 11, the freshly spray-dried IDMC with MMPC exhibited typical amorphous characteristics and no XRD diffraction peaks were detected. The amorphous form of IDMC/MMPC solid dispersions showed superior stability under severe storage conditions. No crystal growth could be detected by XRD after the storage tests for one week, one month, three and six months. The XRD patterns of samples after storage were same as that of the fresh sampleswith typical diffraction patterns of amorphous form. No X-ray diffraction peaks assigned to the crystalline form of IDMC could be observed. The nanospace between the pore channels of MMPC confined IDMC molecules in the amorphous state within the solid dispersion. In addition, the uniform carbon pore walls perfectly separate the fine amorphous particles of IDMC and prevent the re-crystallization and crystal growth even under severe storage conditions, thus enabling the solid dispersion to exhibit excellent amorphous stability. By co-spray drying, only a small amount IDMC stayed on the surface of MMPC submicron particles. On the modified surface of MMPC

containing hydroxyl groups and other oxygen containing groups, the hydrogen bonds between IDMC and surface of MMPC are also believed to limit the movement and crystallization of IDMC on the external surface. This shows a distinct property of MMPC as drug carriers for the formulation of poorly water-soluble drugs. It has also been reported that amorphous APIs of poorly soluble drugs can be obtained by formulation with soluble polymer to form solid dispersions. However, the stability of the amorphous state is often a challenge as re-crystallization occurs due to the low surface areas of polymer [37,38,41-43]. Although a number of formulation methods have been reported to improve the dissolution rate of IDMC, very few reports investigate their stability on storage [44,45]. In this study, the co-spray drying with MMPC not only produces amorphous IDMC as solid dispersions, but also stabilized the amorphous state of IDMC under severe storage condition for six months. The stability of the amorphous state of co-spray dried IDMC/MMPC mono-dispersed solid dispersions was also confirmed by DSC analysis.

4. Conclusions

By co-spray drying sucrose to fill the ordered pore channels of SBA-15 submicron particles with optimized sucrose/SBA-15 ratios of 1.0 ~1.5, well monodispersed mesoporous carbon submicron particles were harvested by subsequent carbonization in a N_2 environemnt at 900 °C followed by the removal of the mesoporous silica hard templates in NaOH solution. The wettability of monodispersed mesoporous carbon was improved by treatment with nitric acid and created oxygen-containing groups on its surface. MMPC was used as drug carrier to encapsulate model poorly soluble drug, IDMC and MMPC exhibited showed superior

ability to non-porous MSC and AC with non-uniform pores in drug loading by co-spray drying with IDMC. In addition, IDMC entrapped in the ordered pore channels of MMPC is in its amorphous form, which contributed to the enhanced dissolution rate. Due to the confined space between the uniform pore walls, the amorphous IDMC/MMPC exhibited excellent stability under stress storage conditions as the rigid pore wall effectively prevented any recrystallization. MMPC has the application potential in formulation of other poorly soluble drugs and candidates to achieve enhanced dissolution and bioavailability.

Acknowledgments

This work was generously supported by Institute of Chemical Engineering and Science, Agency of Science Technology and Research (A*STAR), Singapore

References

[1] C.T. Kresege, M.E. Leonowicz, W.J. Roth, J.C. Vartuli, J.S. Beck, Ordered mesoporous molecular sieves synthesized by a liquid-crystal template mechanism, Nature 359 (1992) 710-712.

[2] T. Asefa, Z.M. Tao, Mesoporous silica and organosilica materials - Review of their synthesis and organic functionalization, Can. J. Chem. 90 (2012) 1015-1031.

[3] M. Vallet-Regí, F. Balas, D. Arcos, Mesoporous materials for drug delivery, Angew. Chem. Int. Edit. 46 (2007) 7548–7558.

[4] B. Chen, G. Quan, Z.H. Wang, J.W. Chen, L.N. Wu, Y.H. Xu, G. Li, C.B. Wu, Hollow mesoporous silicas as a drug solution delivery system for insoluble drugs, Powder Technol. 240 (2013) 48–53.

[5] Q. Ye, J.S. Zhao, F.F. Huo, D. Wang, S.Y. Cheng, T.F. Kang, H.X. Dai, Nanosized Au supported on three-dimensionally ordered mesoporous beta-MnO2: Highly active catalysts for the low-temperature oxidation of carbon monoxide, benzene, and toluene, Micropor. Mesopor. Mat. 172 (2013) 20-29.

[6] K.S. Ha, G. Kwak, K.W. Jun, J. Hwang, J. Lee, Ordered mesoporous carbon nanochannel reactors for high-performance Fischer-Tropsch synthesis, Chem. Comm. 49 (2013) 5141-5143.

[7] T. Xue, Z.P. Sun, L. Wei, X. Wang, J.M. Lee, One-step dual template synthesis of platinum on mesoporous carbon nanowires for electrocatalysts. Int. J. Hydrogen Energ. 38 (2013) 2754-2759.

[8] J. Tang, T. Wang, X. Sun, Y.X. Guo, H.R. Xue, H. Guo, M.Z. Liu, X.X. Zhang, J.P. He, Effect of transition metal on catalytic graphitization of ordered mesoporous carbon and Pt/metal oxide synergistic electrocatalytic performance, Micropor Mesopor. Mat. 177 (2013) 105-112.

[9] D.P. Xu, S.H. Yoon, I. Mochida, Y.M. Qiao, Y.G. Wang, L.C. Ling, Synthesis of mesoporous carbon and its adsorption property to biomolecules, Micropor Mesopor. Mat. 115 (2008) 461-468.

[10] N.F. Nejad, E. Shams, M.K. Amini, J.C. Bennett, Ordered mesoporous carbon CMK-5 as a potential sorbent for fuel desulfurization: Application to the removal of dibenzothiophene and comparison with CMK-3. Micropor Mesopor. Mat. 168 (2013) 239-246.

[11] Z.B. Lei, D. Bai, X.S. Zhao, Improving the electrocapacitive properties of mesoporous CMK-5 carbon with carbon nanotubes and nitrogen doping, Micropor. Mesopor. Mat. 147 (2012) 86-93.

[12] X. He, P. Ling, J. Qiu, M. Yu, X. Zhang, C. Yu, M. Zheng, Efficient preparation of biom-ass-based mesoporous carbons for supercapacitors with both high energy density and high power density, J. Power Sources 240 (2013) 109-113.

[13] Y. Yan, Q. Cheng, V. Pavlinek, P. Saha, C. Li, Controlled synthesis of mesoporous carbon nanosheets and their enhanced supercapacitive performance, J. Solid State Electr. 17 (2013) 1677-1684.

[14] L. Yang, L.R. Hou, Y.W. Zhang, C.Z. Yuan, Facile synthesis of mesoporous carbon nanofibres towards high-performance electrochemical capacitors, Mater. Lett. 97 (2013) 97-99.

[15] X.M. Ma, M.X., Liu, L.H. Gan, Y.H. Zhao, L.W. Chen, Synthesis of micro- and mesoporous carbon spheres for supercapacitor electrode, J. Solid State Electr. 17 (2013) 2293-2301.
[16] J.C. Ndamanisha, L.P. Guo, Ordered mesoporous carbon for electrochemical sensing: A review, Anal. Chim. Acta 747 (2012) 19-28.
[17] C.D. Liang, Z.J. Li, S. Dai, Mesoporous carbon materials: Synthesis and modification, Angew. Chem. Int. Edit. 47 (2008) 3696-3717.
[18] S.H. Joo, S. Jun, R. Ryoo, Synthesis of ordered mesoporous carbon molecular sieves CMK-1, Micropor Mesopor. Mat. 44 (2001) 153-158.
[19] C. Karavasili, E.P. Amanatiadou, L, Sygellou, D.K. Giasafaki, T.A. Steriotis, G.C. Charalambopoulou, I.S. Vizirianakis, D.G. Fatouros, Development of new drug delivery system based on ordered mesoporous carbons: characterisation and cytocompatibility studies J. Mater. Chem. B 1 (2013) 3167-3174.
[20] X. Yuan, W. Xing, S.P, Zhuo, Z.H. Han, G.Q. Wang, X.L Gao, Z.F. Yan, Preparation and application of mesoporous Fe/carbon composites as a drug carrier, Micropor. Mesopor. Mat. 117 (2009) 678-684.
[21] S. Ganta, H. Devalapally, A. Shahiwala, M. Amiji, A review of stimuli-responsive nanocarriers for drug and gene delivery, J. Control. Release 126 (2008) 187-204.
[22] S.M. Moghimi, A.C. Hunter, J.C. Murray, Long-circulating and target-specific nanoparticles: Theory to practice, Pharmacol. Rev. 53 (2001) 283-318.
[23] Q.J. He, M. Ma, C.Y. Wei, J.L. Shi, Mesoporous cabon@silica-silica nanatheranostic for synchronous delivery of insoluble drugs and luminescence imaging. Biomaterials. 33 (2012) 4392-4402.
[24] J.L. Gu, S.S. Su, Y.S. Li, Q.J. He, J.L. Shi, Hydrophilic mesoporous carbon nanoparticles as carriers for sustained release of hydrophobic anti-cancer drugs, Chem. Commun. 47 (2011) 2101-2103.
[25] X.F. Wang, P. Liu, Y. Tian, Ordered mesoporous carbons for ibuprofen drug loading and release behavior, Micropor. Mesopor. Mat. 142 (2011) 334–340.
[26] P. Zhao, L.H, Wang, C.S. Sun, T.Y. Jiang, J.H. Zhang, Q. Zhang, J. Sun, Y.H, Deng, S.L. Wang, Uniform mesoporous carbon as a carrier for poorly water soluble drug and its cytotoxicity study, Eur. J. Pharm. Biopharm. 80 (2012) 535-543.
[27] A. Labiano, M.Z. Dai, D. Taylor, W.S. Young, T.H. Epps, K. Rege, B.D. Vogt, Slow release kinetics of mitoxantrone from ordered mesoporous carbon films. Micropor. Mesopor. Mat. 160 (2012) 143-150.
[28] A. Vinu, K.Z. Hossian, P. Srinivasu, M. Miyahara, S. Anandan, N. Gokulakrishnan, T. Mori, K. Ariga, V.V. Balasubramanian, Carboxy-mesoporous carbon and its excellent adsorption capability for proteins, J. Mater. Chem. 17 (2007), 1819-1825.
[29] S.N. Che, A.E. Garcia-Bennett, X.Y. Liu, R.P. Hodgkins, P.A. Wright, D.Y. Zhao, O. Terasaki, T. Tatsumi, Synthesis of large-pore Ia(3)d mesoporous silica and its tubelike carbon replica, Angew. Chem. Int. Edit. 42 (2003) 3930-3934.
[30] J.J, Li, Y. Liang, B.J. Dou, C.Y. Ma, R.J. Lu, Z.P. Hao, Q. Xie, Z.Q. Luan, K. Li, Nanocasting synthesis of graphitized ordered mesoporous carbon using Fe-coated SBA-15 template, Mater. Chem. Phys. 138 (2013) 484-489.
[31] C.C. Ting, H.Y. Wu, S. Vetrievel, D. Saikia, Y.C. Pan, G.T.K. Fey, H.M. Kao, A one-pot route to synthesize highly ordered mesoporous carbons and silicas

through organic–inorganic self-assembly of triblock copolymer, sucrose and silica, Micropor. Mesopor. Mat. 128 (2010) 1-11.
[32] J. Kastner, T. Pichler, H. Kuzmany, S. Curran, W. Blau, D.N. Weldon, M. Delamesiere, S. Draper, H. Zandbergen, Resonance Raman and infrared spectroscopy of carbon nanotubes, Chem. Phys. Lett. 221 (1994) 53-58.
[33] R.M. Silverstein, G.C. Bassler, T.C. Morrill, Spectrometric Identification of Organic Compounds. fourth ed., John Wiley and Sons, New York, 1981.
[34] P.A. Bazula, A.H. Lu, J.J. Nitz, F. Schüth, Surface and pore structure modification of ordered mesoporous carbons via a chemical oxidation approach, Micropor. Mesopor. Mat. 108 (2008) 266–275.
[35] M. Sliwinska-Bartkowiak, G. Dudziak, R. Gras, R. Sikorski, R. Radhakrishnan, K.E. Gubbins, Freezing behavior in porous glasses and MCM-41. Colloid Surface. A 187-188 (2001) 523-529.
[36] S.C. Shen, W.K. Ng, L. Chia, Y.C. Dong, R.B.H. Tan, Stabilized amorphous state of ibuprofen by co-spray drying with mesoporous SBA-15 to enhance dissolution properties, J. Pharm. Sci. 99 (2010) 1997-2007.
[37] R.T.Y. Lim, W.K. Ng, R.B.H. Tan, Amorphization of pharmaceutical compound by co-precipitation using supercritical anti-solvent (SAS) process (Part I), J. Supercrit. Fluid. 53 (2010) 179-184.
[38] R.T.Y. Lim, W.K. Ng, E. Widjaja, R.B.H. Tan, Comparison of the physical stability and physicochemical properties of amorphous indomethacin prepared by co-milling and supercritical anti-solvent co-precipitation, J. Supercrit. Fluid. 79 (2013) 186-201.
[39] Y.Z. Zhang, H. Wang, C.Q, Gao, X. Li, L.S, Li, Highly ordered mesoporous carbon nanomatrix as a new approach to improve the oral absorption of the water-insoluble drug, simvastatin, Eur. J. Pharm. Sci. 49 (2013) 864-872.
[40] X. Niu, L. Wan, Z. Hou, T.Y. Wang, C.S. Sun, J. Sun, P. Zhao, T.Y. Jiang, S.L. Wang, Mesoporous carbon as a novel drug carrier of fenofibrate for enhancement of the dissolution and oral bioavailability, Int. J. Pharm. 452 (2013) 382–389.
[41] P.J. Marsac, H. Konno, A.C. Rumondor, L.S. Taylor, Recrystallization of nifedipine and felodipine from amorphous molecular level solid dispersions containing poly(vinylpyrrolidone) and sorbed water. Pharm. Res. 25 (2008) 647-656.
[42] M.C. Martinez-Ohárriz, C. Rodríguez-Espinosa, C. Martín, M.M. Goñi, M.C. Tros-Ilarduya, M. Sánchez, Solid dispersions of diflunisal-PVP: Polymorphic and amorphous states of the drug. Drug Dev. Ind. Pharm. 28: 717-725.
[43] S.M. Wong, I.W. Kellaway, S. Murdan, Enhancement of the dissolution rate and oral absorption of a poorly water soluble drug by formulation of surfactant-containing microparticles, Int. J. Pharm. 317 (2006) 61-68.
[44] H.J. Liu, P. Wang, X.Y. Zhang, F. Shen, C.G. Gogos, Effects of extrusion process parameters on the dissolution behavior of indomethacin in Eudragit® E PO solid dispersions, Int. J. Pharm. 383 (2010) 161–169.
[45] A. Sivert, V. Bérard , C. Andrès , New binary solid dispersion of indomethacin with surfactant polymer: From physical characterization to in vitro dissolution enhancement, J. Pharm. Sci. 99 (2010) 1399-1413.

Table 1. Surface and pore properties of monodispersed mesoporous carbon

	Sucrose/SBA-15 ratio	Specific surface areas (m^2/g)	Total pore volume (<55 nm) (cm^3/g)	Micropore volume (<1.5 nm) (cm^3/g)	Pore diameter (nm)
MMPC-1	0.5	1100.8	1.09	0.42	3.8
MMPC-2	1.0	1850.9	1.47	0.67	3.8
MMPC-3	1.5	1825.8	1.82	0.65	3.8
MMPC-4	2.0	1801.5	1.36	0.63	3.4

Figure Captions

Figure 1. (A) Nitrogen adsorption and desorption isotherms for MMPC-1, MMPC-2, MMPC-3 and MMPC-4; (B) Pore size distribution of MMPC-1, MMPC-2, MMPC-3 and MMPC-4.

Figure 2. SEM imagines of MMPC-1, MMPC-2, MMPC-3 and MMPC-4 with a high resolution inset of MMPC-1.

Figure 3. TEM images of MMPC-1, MMPC-2, MMPC-3 and MMPC-4 with high resolution images of MMPC-3 and MMPC-4.

Figure 4. Raman spectra of MMPC-2 and MMPC-3.

Figure 5. FTIR spectra of MMPC-3 and chemically oxidized MMPC-3.

Figure 6. DVS sorption isotherms for the (a) adsorption of Ox-MMPC-3 and (b) desorption of Ox-MMPC-3, (c) adsorption of MMPC-3 and (d) desorption of MMPC-3.

Figure 7. SEM micrographs of MMPC, co-spray dried IDMC/MMPC, MSC, co-spray dried IDMC/MSC, AC and co-spray dried IDMC/AC.

Figure 8. N_2 adsorption isotherms of AC, co-spray dried IDMC/AC, MMPC, co-spray dried IDMC/MMPC, MSC and co-spray dried IDMC/MSC.

Figure 9. DSC curves of co-spray dried IDMC/MMPC, IDMC/AC, IDMC/MSC and pure untreated IDMC crystals.

Figure 10. Dissolution profiles of co-spray dried IDMC/MMPC and compared with pure IDMC crystals

Figure 11. XRD patterns of co-spray dried IDMC/MMPC for (a) fresh sample, and after storage at 40 ^{o}C/75 %RH for (b) one week, (c) one month, (d) three months and (e) six months.

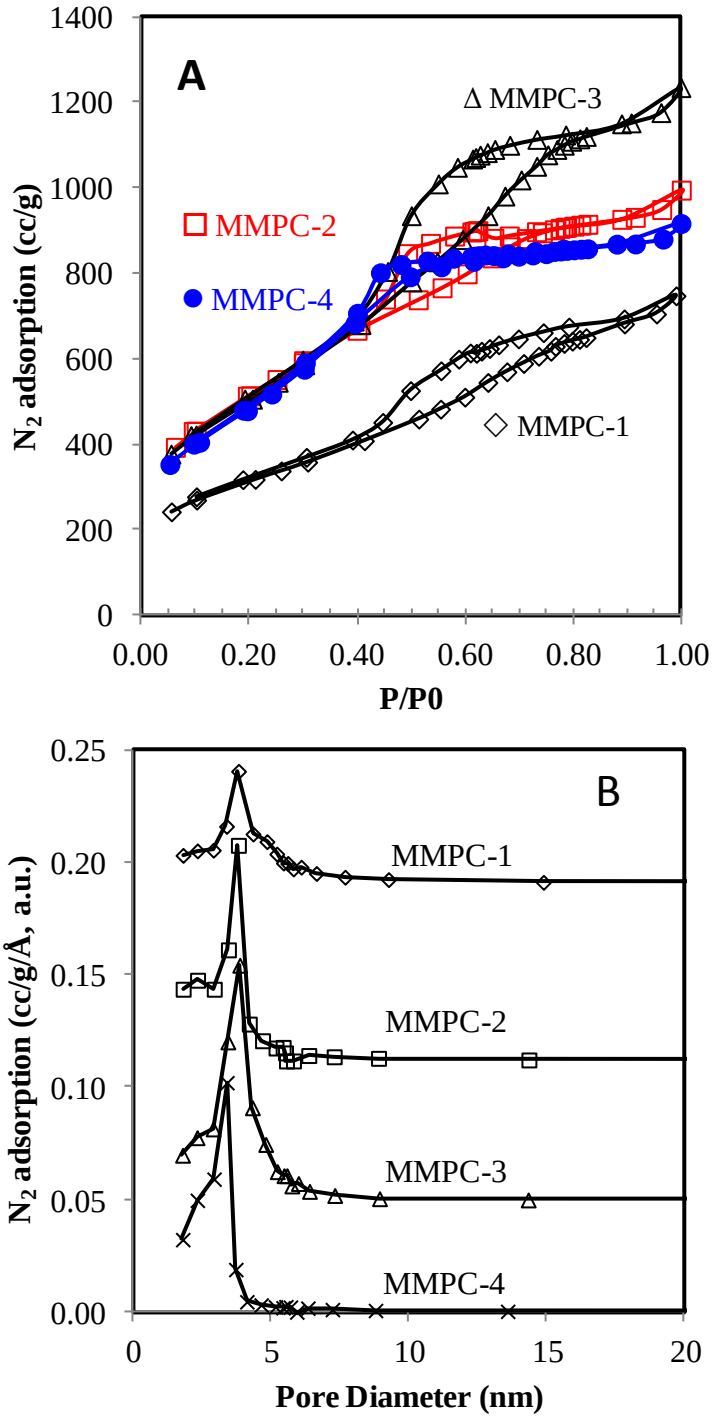

Figure 1. (A) Nitrogen adsorption and desorption isotherms for MMPC-1, MMPC-2, MMPC-3 and MMPC-4; (B) Pore size distribution of MMPC-1, MMPC-2, MMPC-3 and MMPC-4.

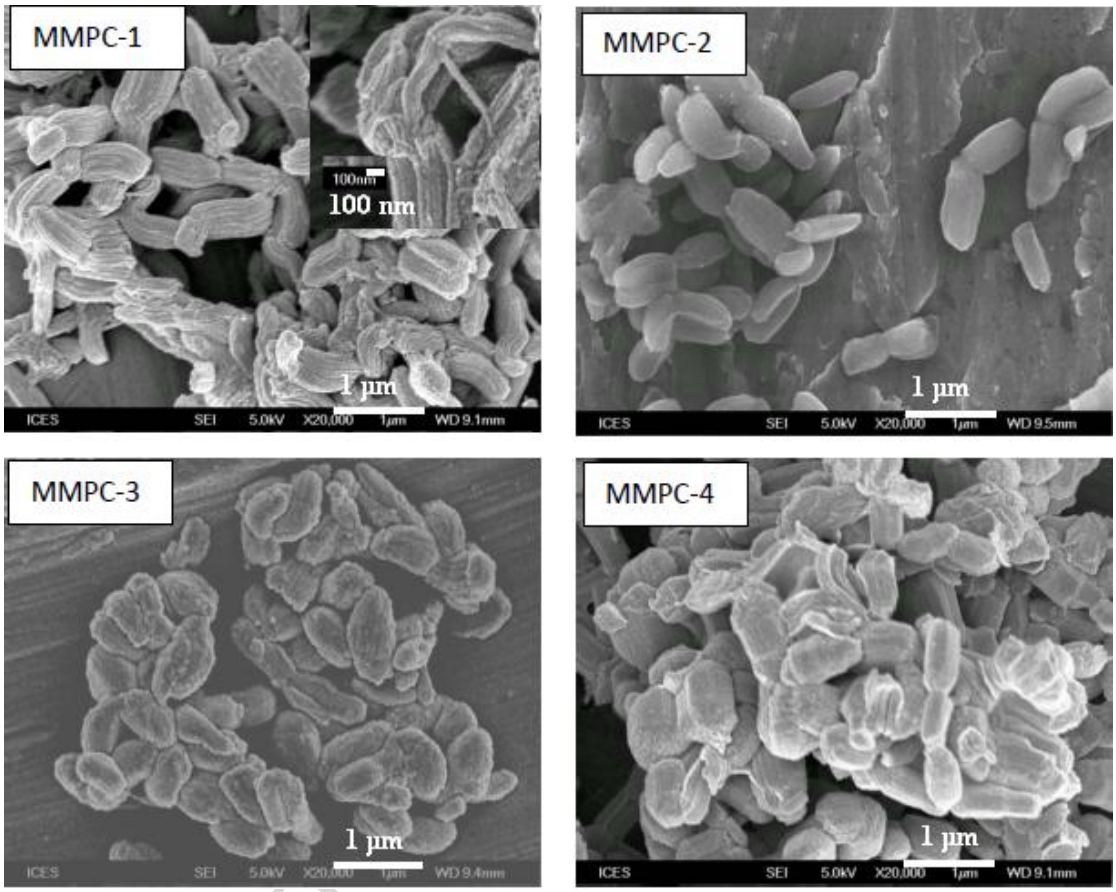

Figure 2. SEM imagines of MMPC-1, MMPC-2, MMPC-3 and MMPC-4 with a high resolution inset of MMPC-1.

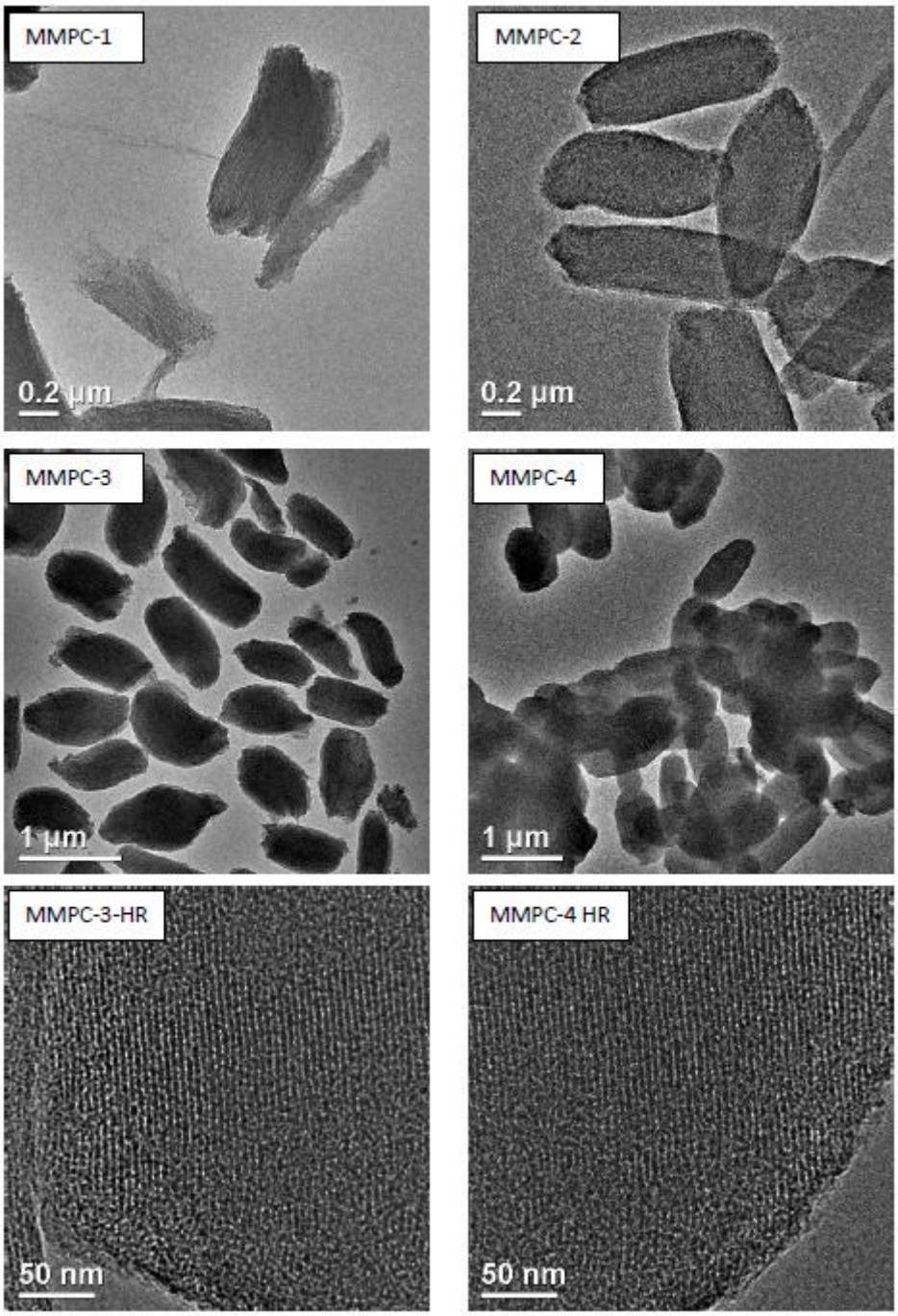

Figure 3. TEM images of MMPC-1, MMPC-2, MMPC-3 and MMPC-4 with high resolution images of MMPC-3 and MMPC-4.

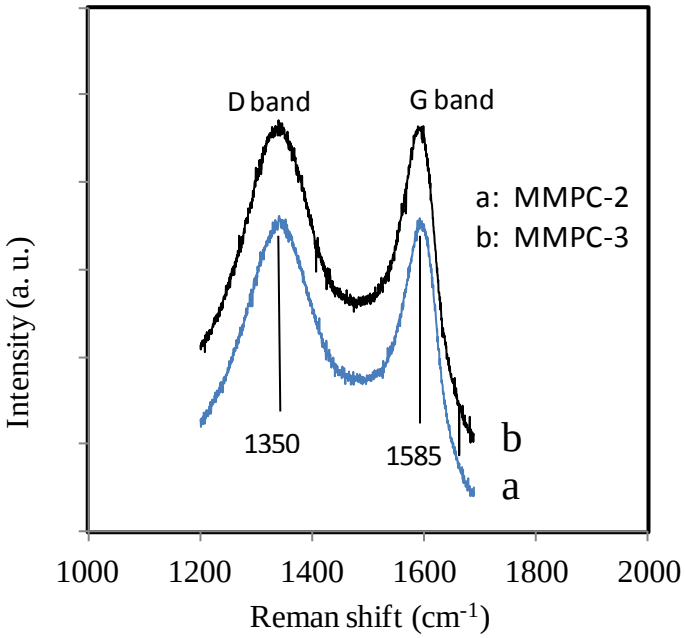

Figure 4. Raman spectra of MMPC-2 and MMPC-3.

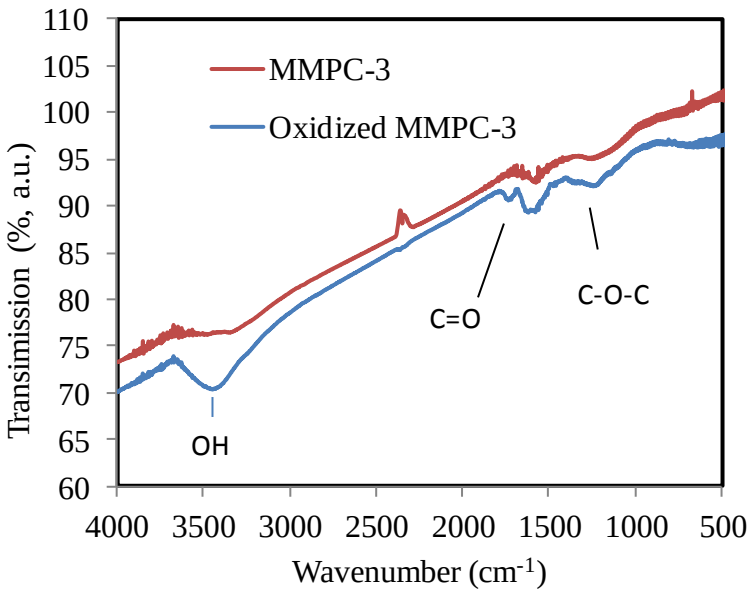

Figure 5. FTIR spectra of MMPC-3 and chemically oxidized MMPC-3.

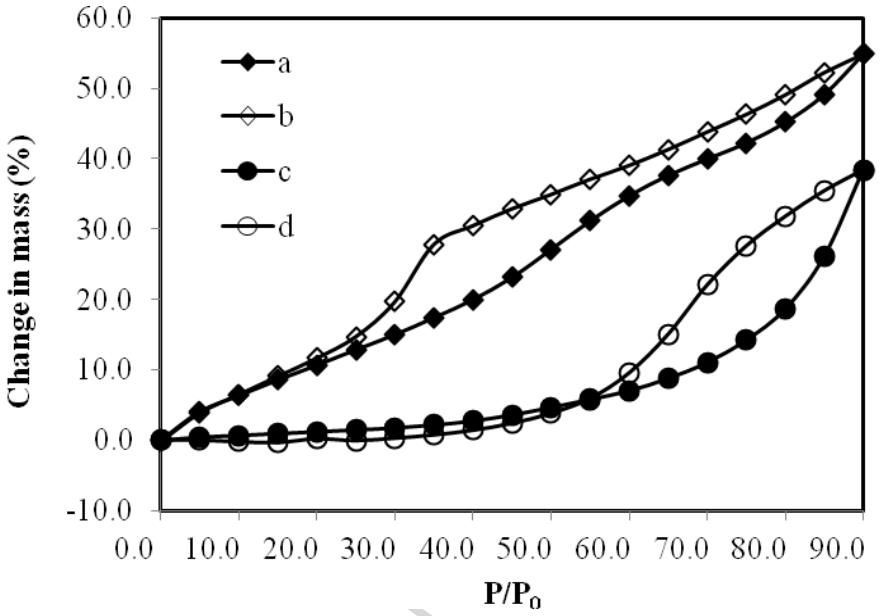

Figure 6. DVS sorption isotherms for the (a) adsorption of Ox-MMPC-3 and (b) desorption of Ox-MMPC-3, (c) adsorption of MMPC-3 and (d) desorption of MMPC-3

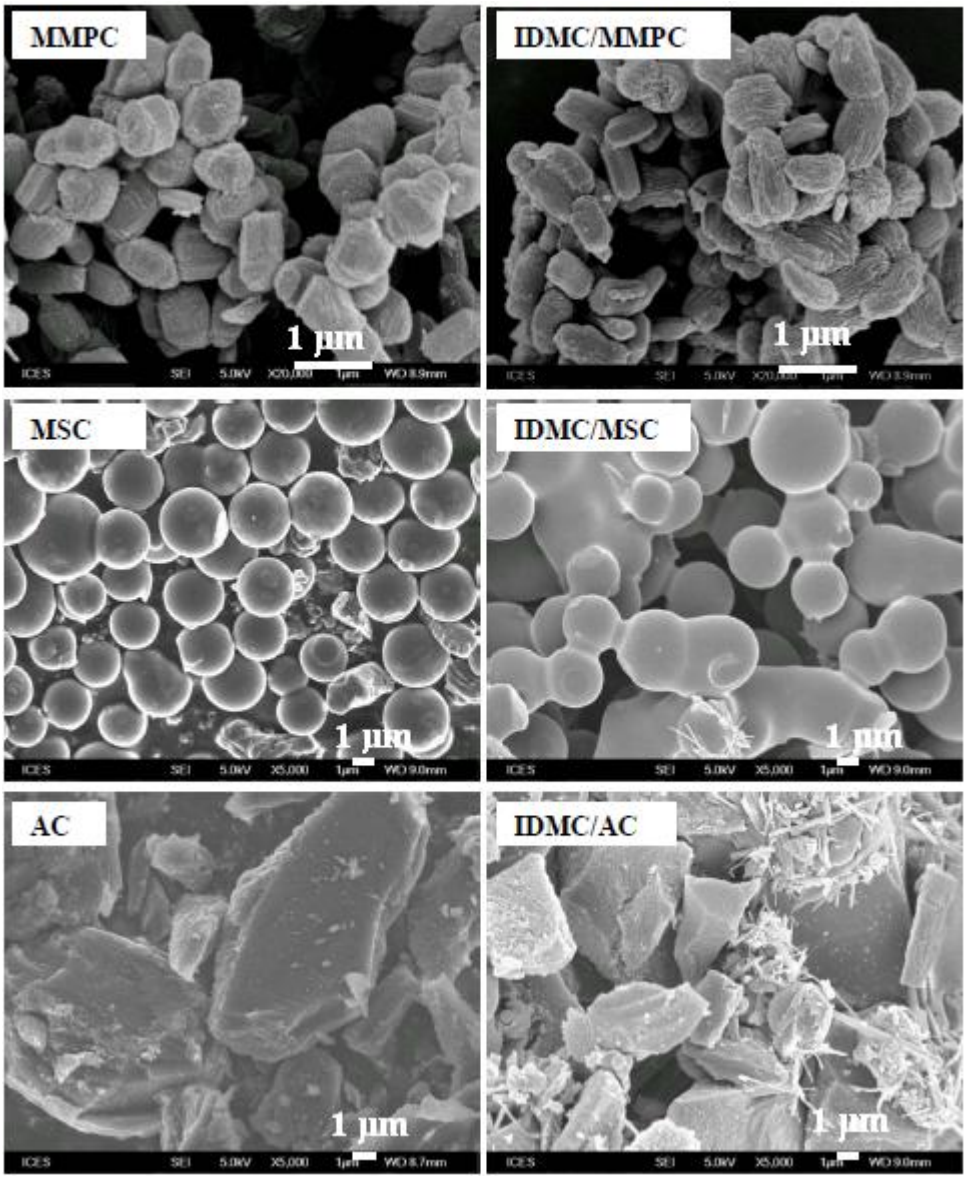

Figure 7. SEM micrographs of MMPC, co-spray dried IDMC/MMPC, MSC, co-spray dried IDMC/MSC, AC and co-spray dried IDMC/AC.

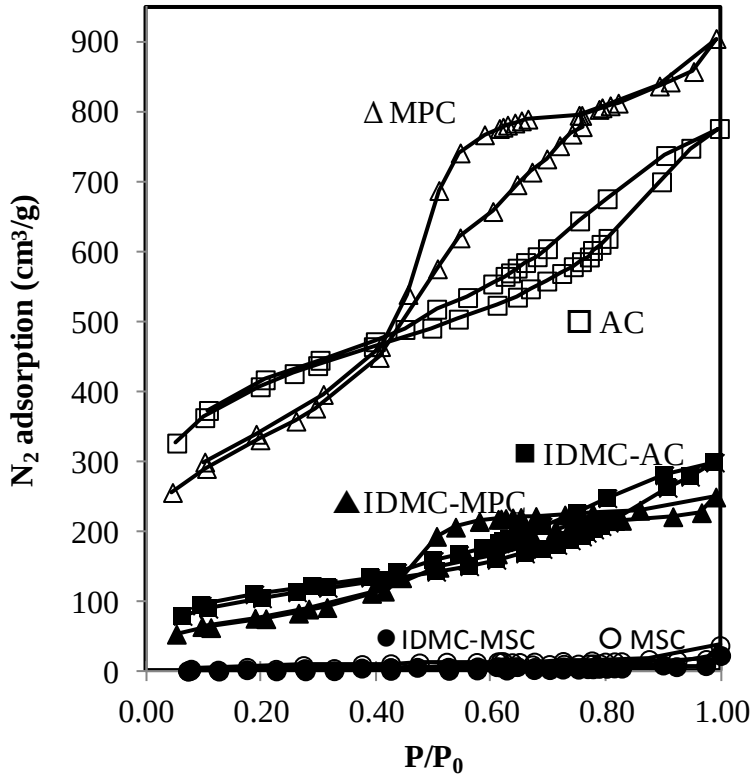

Figure 8. N_2 adsorption isotherms of AC, co-spray dried IDMC/AC, MMPC, co-spray dried IDMC/MMPC, MSC and co-spray dried IDMC/MSC.

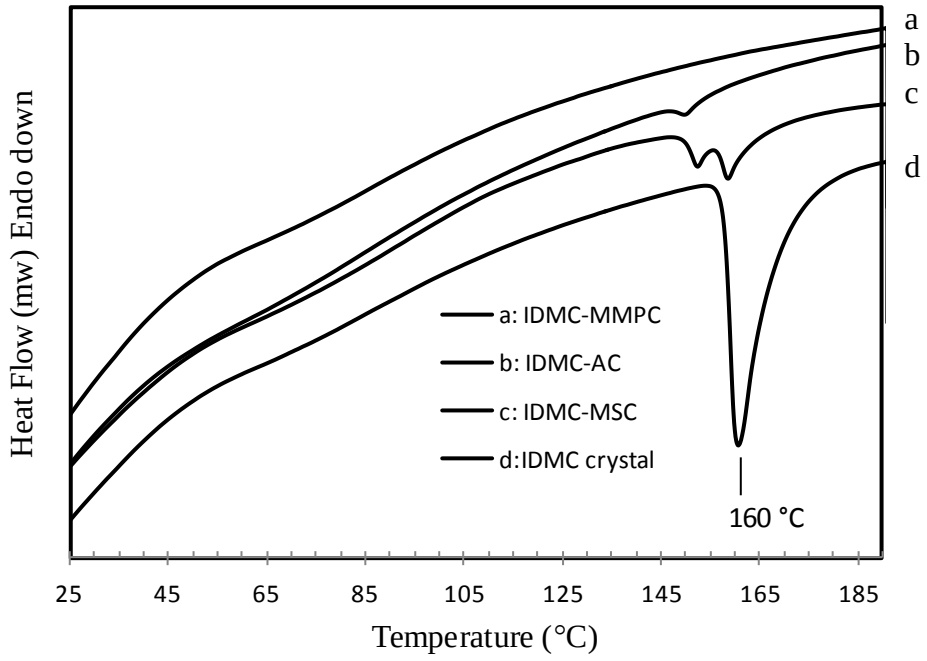

Figure 9. DSC curves of co-spray dried IDMC/MMPC, IDMC/AC, IDMC/MSC and pure untreated IDMC crystals.

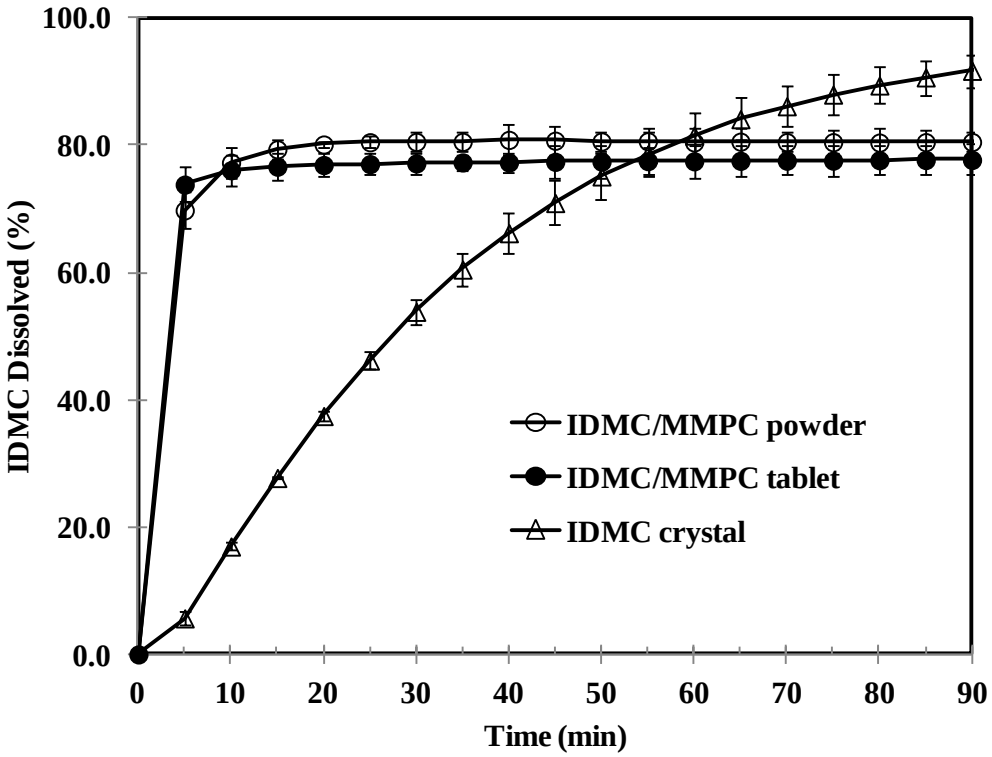

Figure 10. Dissolution profiles of co-spray dried IDMC/MMPC and compared with pure IDMC crystals.

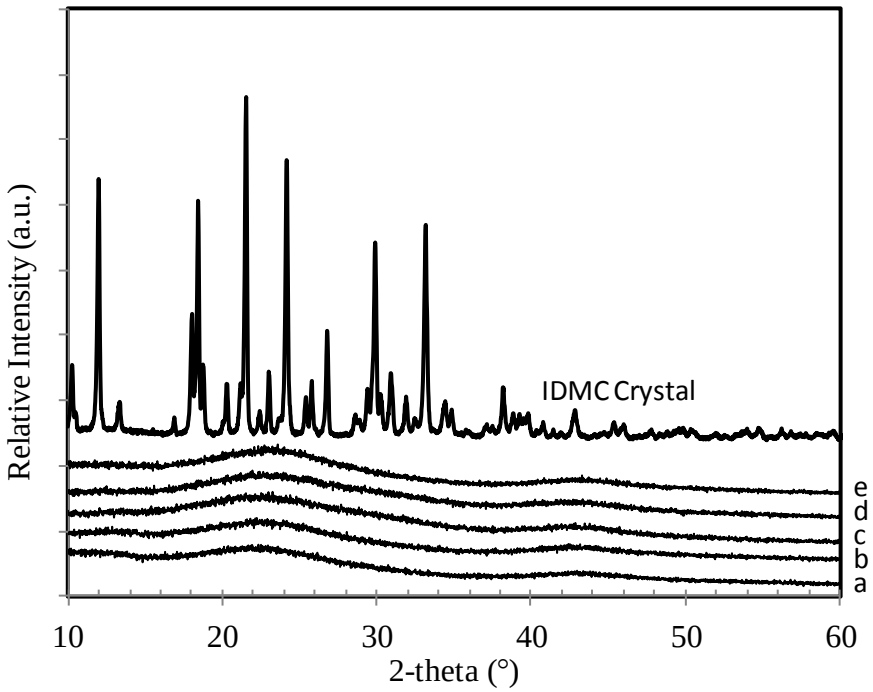

Figure 11. XRD patterns of co-spray dried IDMC/MMPC for (a) fresh sample, and after storage at 40 ^{o}C/75 %RH for (b) one week, (c) one month, (d) three months and (e) six months.

Graphical abstract

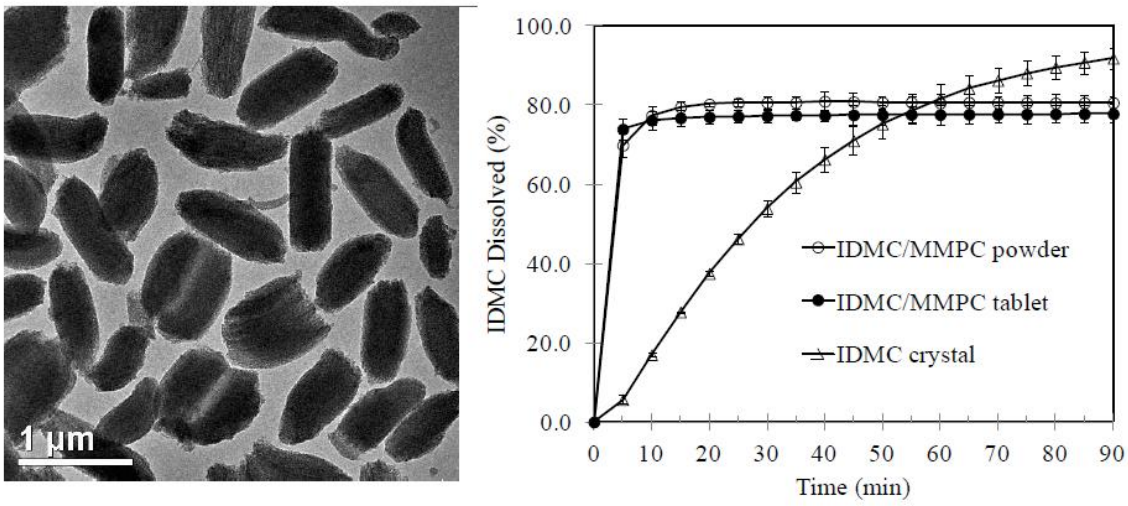

Highlights

- Monodispersed mesoporous carbon (MMPC) submicron particles were successfully fabricated.
- The wettability of mesoporous carbon powder was improved by treatment of surface oxidation.
- The dissolution rate of poorly soluble indomethacin was enhanced by co-spray drying with MMPC.
- The amorphous form of indomethacin in confined nano-space exhibited excellent stability